EXPERIMENTAL STUDY OF OPEN- AND CLOSED-LOOP CONTROL OF A TURBULENT MIXING LAYER

Vladimir Parezanović[1], Jean-Charles Laurentie [1], Carine Fourment [1], Joël Delville [1], Laurent Cordier [1] & Bernd R. Noack [1]
[1]*Institute PPRIME, CNRS, Poitiers, France*

Abstract Open and closed-loop control of a turbulent mixing layer is experimentally performed in a dedicated wind-tunnel facility (TUCOROM). The flow is manipulated with fluidic micro-valve actuators integrated in the trailing edge of the splitter plate. Sensing is performed using a rake of hot-wire probes located downstream in the mixing layer. The control goal is manipulation of the spreading rate and of the virtual origin of the mixing layer. The underlying physical mechanisms employ a wide range of frequencies as well as a wide range of spanwise modes. The calculated Reynolds number based on vorticity thickness is about $Re = 2000$. Control authority is presented with PIV and hot-wire results.

EXPERIMENTAL SETUP AND MEASUREMENTS

The mixing layer is composed of two independent streams generated by the wind tunnel, specifically built for the purpose of this experiment. The two streams meet at the end of a splitter plate which is $8cm$ thick at the start, and $3mm$ at the trailing edge. The tapper is introduced only on the lower side of the splitter plate which is angled at $8°$, while the upper surface is horizontal. The trailing edge contains 96 circular cross section nozzles of $\phi = 2mm$ along its span, which are connected to micro valve actuators. The actuators are capable of frequencies higher than $800Hz$ and of exit velocities of the order of the convection velocity of the mixing layer flow. Each of the micro valves can be controlled separately. Measurements comprise Particle Image Velocimetry (PIV) using two Lavision Image Pro PIV cameras with an acquisition rate of $5Hz$, and local velocity measurements using a rake of 24 hot wire probes. Each camera produces 1200 image pairs of 1040×1376 pixels which cover a combined area of $420mm \times 302mm$, with a 10% overlap. The hot wire probes are placed at $x = 800mm$. The vertical portion of the mixing layer which is covered by the hot wire rake is about two times the local vorticity thickness of the baseline flow. The system used for control is an "iHawk" real time acquisition/processing system capable of acquisition rates up to $200kHz$, with 128 analog input channels, 96 digital input/output channels and 32 analog output channels. The system is capable of closing the input-processing-output loop in less than $20\mu s$.

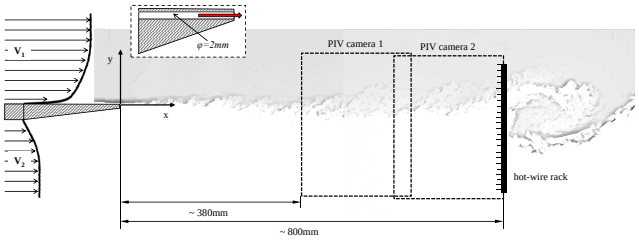

Figure 1. Sketch of the experimental setup. The disposition of the micro jet nozzles is shown in the inset.

RESULTS AND DISCUSSION

The inlet velocities of $U_1 = 9.3m/s$ in the upper and $U_2 = 2.1m/s$ in the lower vein, correspond to a velocity ratio $r = 0.225$. These inlet flow conditions initiate turbulent boundary layers on both sides of the splitter plate of $\delta_{99(1)} = 14.2mm$ and $\delta_{99(2)} = 11.5mm$. Based on the sum of momentum thicknesses at the trailing edge and the trailing edge height, we can estimate the Reynolds number as $Re_{\theta_i} \approx 2000$. The natural frequency of the main instability measured at the position of the hot wire rake is $f_0 \approx 11Hz$. The preliminary results presented here aim at confirming the control authority and establishing a relevant criterion for a state-detection feedback signal. The micro jets are actuating on the spanwise mode 0; all of them are activated in unison, therefore limiting the forcing to mainly 2D dynamics of the mixing layer. The actuation duty cycle is set at 50% and the effects are explored for a range of actuation frequencies, from $5Hz$ to $400Hz$. The most impressive results can be observed for two cases of actuation at low $f_{act} = \approx f_0$ and intermediate $f_{act} \approx 6 \times f_0$ frequencies. Power spectra maps of the velocity time series from all 24 hot wire probes are shown in figure 2. The spectral analysis indicates a frequency synchronization for the low frequency actuation and a global damping of the

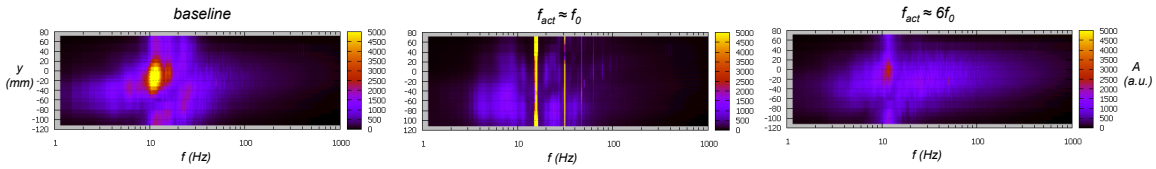

Figure 2. Plot of power spectra maps from the hot wire rake, with each probe absolute position marked on the vertical axis, horizontal axis is the frequency, and the color map shows the intensity of the amplitude of the spectrum in arbitrary units.

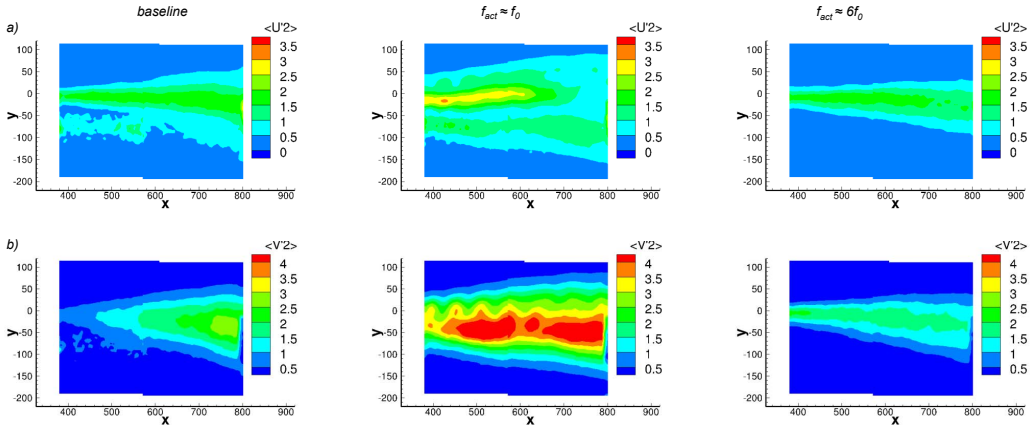

Figure 3. The velocity field mean fluctuations in $(m/s)^2$ for (a) $\overline{u'^2}$ and (b) $\overline{v'^2}$. Columns denote baseline, $f_{act} \approx f_0$ and $f_{act} \approx 6f_0$ cases.

amplitude for the intermediate. The velocity field mean fluctuations $\overline{u'^2}$ and $\overline{v'^2}$ are shown in figure 3 for the three cases. The case of $f_{act} \approx f_0$ shows a strong increase in both vertical and streamwise fluctuations, while $f_{act} \approx 6f_0$ causes the fluctuations to be damped and confined to a much smaller region, even compared to the baseline flow. Proper Orthogonal Decomposition (POD) of the hot wire signals in real time, can provide efficient feedback information. Figure 4 shows a plot of time evolution of POD coefficients $a_n(t)$ projected on the POD eigenvectors basis of the baseline flow, for the four most energetic modes of the three cases investigated above. In comparison with the baseline, we can immediately notice the periodic behavior and synchronization of the second POD mode for $f_{act} \approx f_0$, while $f_{act} \approx 6f_0$ case shows damped oscillations across all modes. These results point to the second POD mode as a likely indicator of the current flow state. A complete investigation of the whole range of frequencies has been performed but is beyond the scope of this abstract. The results reveal three main effects: for $f_0 \leq f_{act} \leq 2f_0$ the effect of synchronization; for $2f_0 \leq f_{act} \leq 10f_0$ a damping effect; and for $f_{act} > 10f_0$ effect of relaxation, ie. gradual return to dynamics similar to the baseline flow. The low frequency excitation increase strongly the fluctuations while the intermediate frequencies dampen them out, hence, we can control the spreading and mixing processes in both directions. The second POD mode proves to be sufficiently robust in it's reaction to flow actuation throughout the whole range of frequencies investigated, and will be used as the closed-loop feedback sensor information.

This project is partially funded by the ANR Chair of Excellence TUCOROM.

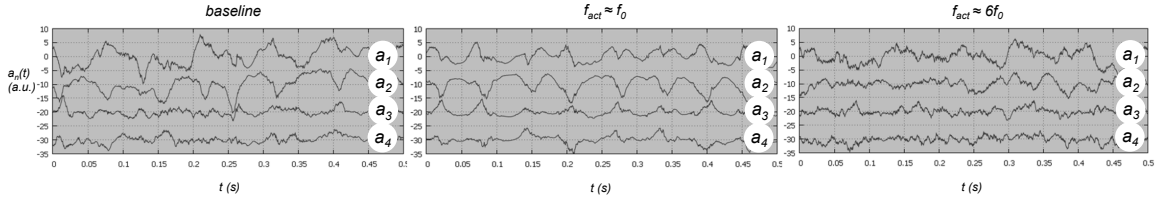

Figure 4. Time evolution of POD mode coefficients $a_n(t)$ for the first four POD modes, for the three cases investigated. Amplitude is shown in arbitrary units and is shifted by $-10a.u.$ for each mode.